CORE
Metadata, citation and similar papers at core.ac.uk
Provided by Caltech Authors - Main

JACS
JOURNAL OF THE AMERICAN CHEMICAL SOCIETY

Caltech Library

Subscriber access provided by Caltech Library

Communication

Nitrogen Fixation via a Terminal Fe(IV) Nitride

Niklas B. Thompson, Michael T. Green, and Jonas C. Peters

J. Am. Chem. Soc., **Just Accepted Manuscript** • DOI: 10.1021/jacs.7b09364 • Publication Date (Web): 09 Oct 2017

Downloaded from http://pubs.acs.org on October 10, 2017

Just Accepted

"Just Accepted" manuscripts have been peer-reviewed and accepted for publication. They are posted online prior to technical editing, formatting for publication and author proofing. The American Chemical Society provides "Just Accepted" as a free service to the research community to expedite the dissemination of scientific material as soon as possible after acceptance. "Just Accepted" manuscripts appear in full in PDF format accompanied by an HTML abstract. "Just Accepted" manuscripts have been fully peer reviewed, but should not be considered the official version of record. They are accessible to all readers and citable by the Digital Object Identifier (DOI®). "Just Accepted" is an optional service offered to authors. Therefore, the "Just Accepted" Web site may not include all articles that will be published in the journal. After a manuscript is technically edited and formatted, it will be removed from the "Just Accepted" Web site and published as an ASAP article. Note that technical editing may introduce minor changes to the manuscript text and/or graphics which could affect content, and all legal disclaimers and ethical guidelines that apply to the journal pertain. ACS cannot be held responsible for errors or consequences arising from the use of information contained in these "Just Accepted" manuscripts.

ACS Publications

Journal of the American Chemical Society is published by the American Chemical Society. 1155 Sixteenth Street N.W., Washington, DC 20036
Published by American Chemical Society. Copyright © American Chemical Society. However, no copyright claim is made to original U.S. Government works, or works produced by employees of any Commonwealth realm Crown government in the course of their duties.

Nitrogen Fixation via a Terminal Fe(IV) Nitride

Niklas B. Thompson,[†] Michael T. Green,*[,‡] Jonas C. Peters*[,†]

[†]Division of Chemistry and Chemical Engineering, California Institute of Technology, Pasadena, California 91125, USA

[‡]Department of Chemistry, University of California – Irvine, Irvine, California 92697, USA

Supporting Information Placeholder

ABSTRACT: Terminal iron nitrides (Fe≡N) have been proposed as intermediates of (bio)catalytic nitrogen fixation, yet experimental evidence to support this hypothesis has been lacking. In particular, no prior synthetic examples of terminal Fe≡N species have been derived from N_2. Here we show that a nitrogen-fixing Fe-N_2 catalyst can be protonated to form a neutral Fe(NNH_2) hydrazido(2−) intermediate, which, upon further protonation, heterolytically cleaves the N–N bond to release $[Fe^{IV}{\equiv}N]^+$ and NH_3. These observations provide direct evidence for the viability of a Chatt-type (distal) mechanism for Fe-mediated N_2-to-NH_3 conversion. The physical oxidation state range of the Fe complexes in this transformation is buffered by covalency with the ligand, a feature of possible relevance to catalyst design in synthetic and natural systems that facilitate multi-proton/multi-electron redox processes.

The chemistry of high valent iron plays a central role in many challenging chemical transformations.[1] For example, the heme oxygenases, as in the cytochrome P450 superfamily, hydroxylate unactivated C–H bonds *via* oxoferryl (Fe^{IV}=O) intermediates derived from the heterolytic reduction of dioxygen ($Fe^{II} + O_2 + 2\ H^+/2\ e^- \rightarrow Fe^{IV}{=}O + H_2O$; Scheme 1**A**).[1-2] The nitrido ion (N^{3-}) is isolobal to the oxo ion (O^{2-}), and by analogy to Fe-mediated catalytic O_2 reduction, we have proposed that Fe-mediated (bio)catalytic nitrogen (N_2) reduction to generate ammonia (NH_3) might proceed heterolytically at a single Fe site ($Fe^I + N_2 + 3\ H^+/3\ e^- \rightarrow Fe^{IV}{\equiv}N + NH_3$; Scheme 1**B**).[3] Such a scenario would be similar to that originally proposed by Chatt for molybdenum-mediated N_2-to-NH_3 conversion,[4] and thought to be operative in the catalytic cycles of known Mo catalysts for this reaction.[5] Whereas terminal Fe≡N complexes have been shown to liberate NH_3 via reductive protonation,[3a, 6] such Fe≡N species have to-date been generated by N-atom transfer reactions from azide (N_3^-) or alternative reagents, not from N_2.[3a, 6-7] Hence, their potential role in synthetic or biological N_2-to-NH_3 conversion catalysis has remained unclear.

Our recent discovery that the anionic N_2 complex $[(P_3^B)Fe(N_2)]^-$ (P_3^B = tris(*o*-diisopropylphosphinophenyl)borane) catalyzes N_2-to-NH_3 conversion has positioned us to probe the mechanism(s) by which the key N–N cleavage step occurs in a catalytically-functional Fe system.[8] Of particular interest has been to distinguish between an early Chatt-type cleavage pathway (a distal mechanism via an Fe≡N intermediate), versus a late-stage cleavage pathway (an alternating mechanism via an Fe–N_2H_4 intermediate).[9] While we have considered the possibility that both scenarios might be viable,[10] a key feature of the tri(phosphine)borane Fe system is its structurally and electronically flexible Fe–B interaction, which allows access to both reduced trigonal bipyramidal Fe(N_2) species as well as, in principle, pseudo-tetrahedral terminal Fe≡N.[11] Here we report the stepwise reduction and protonation of this Fe-based N_2 fixation catalyst to yield a terminal Fe(IV) nitride and NH_3, derived from N_2. This result provides a plausible mechanism for the N–N bond cleavage step under catalytic turnover, and highlights a terminally-bound $Fe^{IV}{\equiv}N$ as a viable intermediate of catalytic N_2 fixation.

Scheme 1.

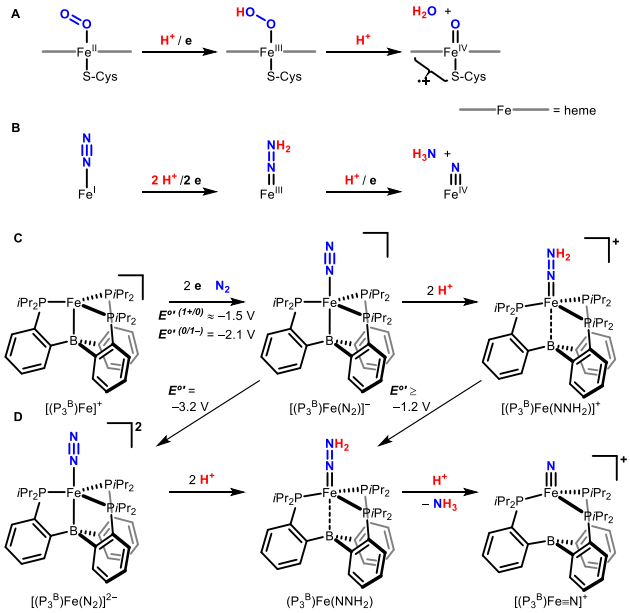

The Fe borane complex $[(P_3^B)Fe(N_2)]^-$, or its oxidized congener $[(P_3^B)Fe]^+$, catalyze the reduction of N_2 to NH_3 at low temperature in diethyl ether (Et_2O) using various acid/reductant combinations, including $HBAr^F{}_4/KC_8$ and $[Ph_2NH_2][OTf]/Cp^*{}_2Co$ ($HBAr^F{}_4$ = $[H(Et_2O)_2][BAr^F{}_4]$; $BAr^F{}_4$ = tetrakis(3,5-bis(trifluoromethyl)phenyl)borate; OTf = trifluoromethanesulfonate; Cp* = pentamethylcyclopentadienide).[8] In a separate synthetic study, it was shown that $[(P_3^B)Fe(N_2)]^-$ reacts rapidly with excess $HBAr^F{}_4$ at very low temperatures to form the cationic hydrazido(2−) complex $[(P_3^B)Fe(NNH_2)]^+$ (Scheme 1**C**; potentials shown are measured in THF vs the ferrocenium/ferrocene couple $[Fc^+/Fc]$).[12] While this protonated complex represents a distal intermediate en route to NH_3, a key question is whether, upon further reduction, a distal mechanism is maintained, or cross-over to an alternating pathway occurs instead.[10, 12] To probe further steps in the catalytic N_2 fixtion mechanism, we therefore sought access to the one-electron reduced hydrazido complex $(P_3^B)Fe(NNH_2)$ to evaluate the viability of N–N bond cleavage via subsequent protonation.

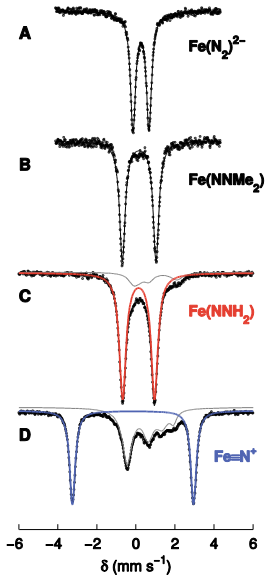

E. Collected Mössbauer parameters

	δ (mm s^{-1})	$\|\Delta E_Q\|$ (mm s^{-1})
$[(P_3^B)Fe(N_2)]^{2-}$ [DFT]	0.26 [0.36(4)]	0.82 [0.8(3)]
$(P_3^B)Fe(NNMe_2)$	0.17	1.73
$(P_3^B)Fe(NNH_2)$ [DFT]	0.14 [0.19(4)]	1.63 [1.7(3)]
$[(P_3^B)Fe{\equiv}N]^+$ [DFT]	−0.15 [−0.21(4)]	6.20 [5.6(3)]

F. Collected EXAFS/XANES data

	Fe–N (Å)	N–N (Å)	Pre-edge (eV (area))
$[(P_3^B)Fe(N_2)]^{2-}$ [DFT]	1.77(2) [1.771]	1.16(2) [1.158]	7112.6 (14) 7114.4 (29) [7113.5 (7) 7114.1 (5)]
$(P_3^B)Fe(NNMe_2)$ {XRD}	1.65(2) {1.680}	1.34(2) {1.293}	7111.4 (15) 7115.5 (29)
$(P_3^B)Fe(NNH_2)$ [DFT]	1.65(2) [1.653]	1.34(2) [1.326]	7111.6 (11) 7115.9 (6) [7111.4 (5) 7115.6 (16)]
$[(P_3^B)Fe{\equiv}N]^+$ [DFT]	1.54(2) [1.514]		7112.1 (87) 7114.3 (5) 7116.7 (14) [7112.0 (65) 7113.9 (5) 7116.7 (17)]

Figure 1. (**A–D**) Collected Mössbauer data; raw data are shown as circles and the simulated data as a solid black line with individual sub-spectra plotted in grey, red, and blue. Full simulation parameters are given in the SI. (**A**) Spectrum of $[(P_3^B)Fe(N_2)]^{2-}$ prepared in situ from $[(P_3^B)Fe(N_2)]^-$. (**B**) Spectrum of $(P_3^B)Fe(NNMe_2)$. (**C**, **D**) Freeze-quench Mössbauer spectra from the reaction of $[(P_3^B)Fe(N_2)]^{2-}$ with excess TfOH, showing conversion to $(P_3^B)Fe(NNH_2)$ (red sub-spectrum, ~ 90%) after mixing for 15 minutes (**C**), and subsequent formation of $[(P_3^B)Fe{\equiv}N]^+$ (blue sub-spectrum, ~ 60%) after mixing for 120 minutes (**D**). Collected Mössbauer and XAS characterization data for these species are given in tables **E** and **F**. N–N distances are calculated by subtraction of Fe–N single scattering paths from a Fe–N–N multiple scattering path.

Preparations of $[(P_3^B)Fe(NNH_2)]^+$ typically contain several Fe-based impurities,[12] so rather than direct reduction of this species, we determined that protonation of the 18 e$^-$ dianionic complex $[(P_3^B)Fe(N_2)]^{2-}$ produces $(P_3^B)Fe(NNH_2)$ most cleanly. Reduction of the $[Na(12\text{-crown-}4)_2]^+$ salt of $[(P_3^B)Fe(N_2)]^-$ with KC_8 in dimethoxyethane (DME) followed by crystallization enables the isolation of $[Na(12\text{-crown-}4)_2][K(DME)_x][(P_3^B)Fe(N_2)]$ as a black solid, featuring an N–N stretching vibration at 1836 cm^{-1}. As $[(P_3^B)Fe(N_2)]^{2-}$ (−3.2 V vs Fc^+/Fc) is more reducing than its alkali metal counterions (e.g. −3.04 V vs Fc^+/Fc for $Na^{+/0}$) in ethereal solvents , it is subject to disproportionation in solution, and such preparations invariably contain $[K(DME)_x][(P_3^B)Fe(N_2)]$ as a contaminant. Thus for all subsequent studies, $[(P_3^B)Fe(N_2)]^{2-}$ was produced in situ and used immediately. The ^{57}Fe Mössbauer spectrum of $[(P_3^B)Fe(N_2)]^{2-}$ produced from the reduction of ^{57}Fe-enriched $[Na(12\text{-crown-}4)_2][(P_3^B)Fe(N_2)]$ (Fig. 1**A**) reveals parameters consistent with its diamagnetic ground state (Fig. 1**E**),[8b] and which are nearly identical with those of the isoelectronic and isostructural silyl complex $[(P_3^{Si})Fe(N_2)]^-$ (P_3^{Si} = tris(*o*-diisopropylphosphinophenyl)silyl).[13]

An in situ prepared sample of ^{57}Fe-enriched $[(P_3^B)Fe(N_2)]^{2-}$ reacted with an excess of either triflic acid (TfOH) or $HBAr^F_4$ in supercooled (i.e. between the glass transition at 91and the freezing point at 137 K) 2-methyltetrahydrofuran (2-MeTHF), and the products were analyzed by Mössbauer spectroscopy. Dianion $[(P_3^B)Fe(N_2)]^{2-}$ reacts cleanly with both acids to form a new species in ca. 90% yield with δ = 0.14 and $|\Delta E_Q|$ = 1.63 mm s^{-1} (Fig. 1**C** and S21**A**) over the course of ~15 min. These parameters are similar to those of the diamagnetic hydrazido complex $[(P_3^{Si})Fe(NNH_2)]^+$ (δ = 0.13 and $|\Delta E_Q|$ = 1.48 mm s^{-1}),[10] and we therefore assign this species as the isoelectronic, isostructural, neutral hydrazido $(P_3^B)Fe(NNH_2)$ in an S = 0 ground state (Scheme 1**D**). Unlike its silyl analog, $(P_3^B)Fe(NNH_2)$ is very thermally sensitive, decomposing in solution within 15 minutes upon warming to 195 K. To further cement our assignment, we prepared the isoelectronic but more stable alkylhydrazido(2−) complex $(P_3^B)Fe(NNMe_2)$ as a spectroscopic model. Alkylhydrazido $(P_3^B)Fe(NNMe_2)$ has been structurally characterized and its Mössbauer spectrum reveals parameters very similar to those observed for $(P_3^B)Fe(NNH_2)$ (Fig. 1**B**, **E**). We note that although the ground state of $(P_3^B)Fe(NNMe_2)$ has S = 0, this alkylhydrazido possesses a low-energy triplet (S = 1) excited state (Fig. S35, Table S14), which is also expected for $(P_3^B)Fe(NNH_2)$ on the basis of computational studies (Table S16).

Mixing $[(P_3^B)Fe(N_2)]^{2-}$ with either acid in excess for longer times produces a new species in the Mössbauer spectrum as the major Fe-containing product (≥ 50% yield with TfOH; Fig. 1**D**, S21**B**), suggesting a product resulting from the decay of $(P_3^B)Fe(NNH_2)$. This new species (δ = −0.15 and $|\Delta E_Q|$ = 6.20 mm s^{-1}) has parameters that are diagnostic for Fe(IV) nitrides under C_3 symmetry,[3b, 6, 7d] and is therefore assigned as the S = 0 nitrido cation $[(P_3^B)Fe{\equiv}N]^+$. Negative isomer shifts are observed for Fe species featuring short, covalent interactions, such as those made with terminal N^{3-} and O^{2-} ligands, which drive Fe *s*-electron density toward the nucleus.[14] The observation of quadrupole splittings > 5 mm s^{-1} is limited to C_3-symmetric Fe complexes featuring Fe≡L triple bonds, which results in an axial polarization of the electric field gradient due to localization of the Fe 3*d* electrons to a δ-symmetry *e* orbital set.[3b, 6, 7d, 15] Thus, the simultaneous observation of a negative δ and $|\Delta E_Q|$ > 6 mm s^{-1} in argues strongly in favor of our assignment of $[(P_3^B)Fe{\equiv}N]^+$, which is also corroborated by XAS studies (*vide infra*). The absence of magnetic hyperfine splitting in spectra of $(P_3^B)Fe(NNH_2)$ and $[(P_3^B)Fe{\equiv}N]^+$ collected at 5 K in the presence of a 50 mT field is consistent with our assignment of non-Kramers spin states.[14] Computational studies reveal a diamagnetic ground state in both cases, and only the S = 0 states accurately reproduce the observed Mössbauer spectroscopic parameters (Fig. 1**E**, Table S16). As with hydrazido $(P_3^B)Fe(NNH_2)$, nitrido $[(P_3^B)Fe{\equiv}N]^+$ is thermally unstable in solution, and degrades upon warming to temperatures ≥ 195 K for longer than 30 minutes to a mixture of $(P_3^B)Fe(OTf)$ and unknown species with parameters consistent with high-spin Fe(II).

To gain additional structural characterization of the thermally unstable complexes $(P_3^B)Fe(NNH_2)$ and $[(P_3^B)Fe{\equiv}N]^+$, we turned to Fe K-edge X-ray absorption spectroscopy. The XANES spectrum of $(P_3^B)Fe(NNH_2)$ features two moderate intensity resonances in the pre-edge region separated by 4.3 eV (Fig. 2**A**). The XANES spectrum of $(P_3^B)Fe(NNMe_2)$ displays two resonances of similar intensity separated by 4.1 eV, but red-shifted by ca. 0.3 eV, consistent with replacement of the *N*-H substituents with more electron rich *N*-Me (Fig. 2**A**, Fig. 1**F**). As observed previously for the C_3-symmetric Fe(IV) nitrides $(PhBP^R_3)Fe(N)$ ($PhBP^R_3$ = $[PhB(CH_2PR_2)_3]^-$; R = *i*Pr, CH_2Cy),[16] the pre-edge XANES spectrum of $[(P_3^B)Fe{\equiv}N]^+$ is dominated by an intense resonance at 7112.1 eV integrating to 87 units (Fig. 2**A**). Based on the purity of the XAS sample (Fig. S25**B**), this integration represents a lower limit of the true intensity of the resonance. This resonance is attributable to a transition from the 1*s* to an a_1-symmetry orbital with significant Fe 4*p* and ligand 2*p* admixture (*vide infra*). This imparts dipole-allowed character to the transition, and is a hallmark of M-to-N/O multiple bonding.[16-17] Furthermore, the pre-edge spectra of $(P_3^B)Fe(NNH_2)$ and $[(P_3^B)Fe{\equiv}N]^+$ predicted by time-dependent density functional theory (TD-DFT) are in very good agreement with those observed experimentally (Fig. 2**B**).

The EXAFS region reveals a short Fe–N bond of 1.65(2) Å in $(P_3^B)Fe(NNH_2)$ (Fig. 2**D**), which compares favorably with that predicted by DFT and observed experimentally for model complex $(P_3^B)Fe(NNMe_2)$ (Fig. 2**C**, Fig. 1**F**). Upon cleavage of the N–N bond in $(P_3^B)Fe(NNH_2)$ to form $[(P_3^B)Fe{\equiv}N]^+$, the Fe–N bond contracts to 1.54(2) Å (Fig. 2**E**, Fig. 1**F**), which is within the range observed in previously characterized C_3-symmetric Fe(IV) nitrides (1.51 to 1.55 Å),[7d, 7e, 16] and shorter than those observed in C_4-symmetric, octahedral Fe(V/VI) nitrides (1.57 to 1.64 Å).[7c, 7g-h] A peak at $R + \Delta$ = 2.5 Å in the Fourier transformed EXAFS of $(P_3^B)Fe(NNH_2)$ and $(P_3^B)Fe(NNMe_2)$, due to an Fe–N–N multiple scattering path, is notably absent in the transform of $[(P_3^B)Fe{\equiv}N]^+$ (Fig. 2**C**–**E**).

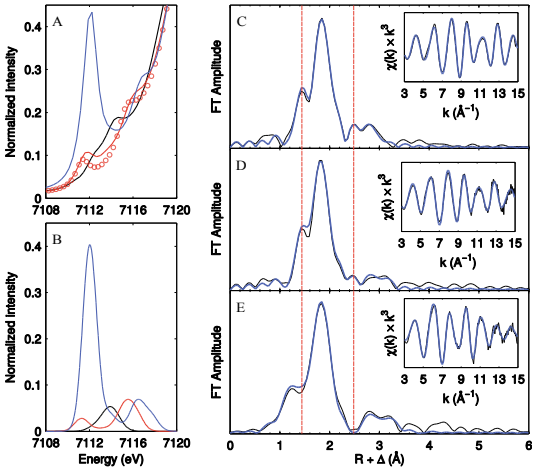

Figure 2. Collected XAS data. (**A**) Pre-edge regions of the XANES spectra of $[(P_3^B)Fe(N_2)]^{2-}$ (black), $(P_3^B)Fe(NNH_2)$ (red), $(P_3^B)Fe(NNMe_2)$ (red circles), and $[(P_3^B)Fe{\equiv}N]^+$ (blue). (**B**) TD-DFT-predicted spectra of $[(P_3^B)Fe(N_2)]^{2-}$ (black), $(P_3^B)Fe(NNH_2)$ (red), and $[(P_3^B)Fe{\equiv}N]^+$ (blue). (**C**–**E**) Phase-uncorrected EXAFS data for (**C**) $(P_3^B)Fe(NNMe_2)$, (**D**) $(P_3^B)Fe(NNH_2)$, and (**E**) $[(P_3^B)Fe{\equiv}N]^+$. The data are plotted in black, with simulations in blue. The k^3-weighted EXAFS oscillations are shown in the inset. The dashed red line at $R + \Delta \sim 1.4$ Å indicates the position of a peak due to an Fe–N scatterer in $(P_3^B)Fe(NNMe_2)$, while that at $R + \Delta$ ~2.5 Å indicates the position of a peak due to an Fe–N–N multiple scatterer. Note that the phase shift, Δ, is typically on the order of 0.4 Å.

Figure 3**A** shows the calculated frontier orbitals of $[(P_3^B)Fe{\equiv}N]^+$, which has the expected $|1e^4(3d_{xy}, 3d_{x^2-y^2})1a_1 2e(3d_{xz}, 3d_{yz})\rangle$ configuration for a C_3 symmetric, formally Fe(IV) nitride.[3a, 7e] The low energy of the virtual $1a_1$ orbital has been explained in terms of (i) an axial distortion which reduces the σ* character of the orbital with respect to the equatorial ligands, and (ii) by 3*d*-4*p* mixing. In $[(P_3^B)Fe{\equiv}N]^+$, the $1a_1$ orbital is additionally stabilized by a bonding interaction with the vacant B $2p_z$ orbital (Fig. 3**B**). A Löewdin population analysis of this orbital reveals nearly equal distribution among the Fe, N, and B atoms, with identical Fe 3*d* (9.5%) and 4*p* (9.1%) character. The significant amount of predicted ligand 2*p* character of this orbital (43%) is consistent with the intensity of the first pre-edge transition observed for $[(P_3^B)Fe{\equiv}N]^+$, which is not expected on the basis of the 3*d*-4*p* mixing alone.[16-18]

Based on these collective data, we propose the sequence of reactions shown in Scheme 1**D**. Rapid protonation of $[(P_3^B)Fe(N_2)]^{2-}$ at low temperature results in formation of hydrazido $(P_3^B)Fe(NNH_2)$ (via presumed diazenido complex $[(P_3^B)Fe(N_2H)]^-$). In a kinetically-slow step, $(P_3^B)Fe(NNH_2)$ is protonated to form an unobserved transient (or transition state) hydrazidium cation $[(P_3^B)Fe(NNH_3)]^+$, which decays *via* heterolytic rupture of the N—N bond to yield NH_3 and $[(P_3^B)Fe{\equiv}N]^+$. In a larger-scale experiment, protonation of $[(P_3^B)Fe(N_2)]^{2-}$ with TfOH in supercooled 2-MeTHF produced NH_3 in 36.0(5)% isolated yield, comparable to the observed yield of $[(P_3^B)Fe{\equiv}N]^+$ under identical conditions (~50% Fig. S24**A**). Under catalytic conditions (i.e. with a reductant present), we propose that $[(P_3^B)Fe{\equiv}N]^+$ can be reduced by 3 H^+/3 e^- to form a second equivalent of NH_3 and $[(P_3^B)Fe]^+$ (or $[(P_3^B)Fe(NH_3)]^+$),[3a, 6] from which $[(P_3^B)Fe(N_2)]^-$ can be regenerated in turn upon reduction.[19] Indeed, sequential reaction of $[(P_3^B)Fe(N_2)]^{2-}$ with TfOH and Cp^*_2Co in supercooled 2-MeTHF doubles the isolated yield of NH_3 to 73(17)%.

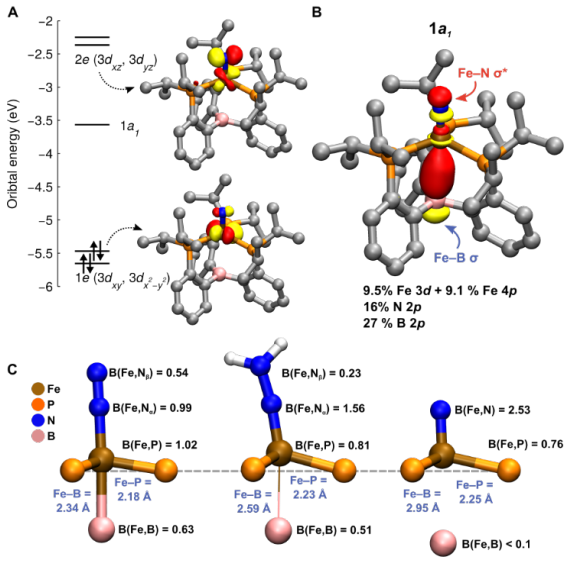

Figure 3. (**A**) Frontier Kohn-Sham orbitals computed for $[(P_3^B)Fe{\equiv}N]^+$. One representative orbital of the filled δ-symmetry 1*e* set and the empty π*-symmetry 2*e* set are presented. (**B**) Löewdin population analysis of the empty $1a_1$ frontier orbital of $[(P_3^B)Fe{\equiv}N]^+$ showing Fe–B σ and Fe–N σ* character. (**C**) Geometric analysis of the bonding in $[(P_3^B)Fe(N_2)]^{2-}$, $(P_3^B)Fe(NNH_2)$, and $[(P_3^B)Fe{\equiv}N]^+$. The Fe–B distances from DFT models are given, along with the average Fe–P bond length from the EXAFS data. Shown in black are the Mayer bond orders (the average in the case of Fe–P).

We have shown that two reductants, KC_8 and Cp^*_2Co, can drive catalytic N_2 fixation in this system, yet only KC_8 is sufficiently reducing to access dianion $[(P_3^B)Fe(N_2)]^{2-}$ under catalytic turnover. The most reduced state of the catalyst accessible with Cp^*_2Co is the anion $[(P_3^B)Fe(N_2)]^-$,[8c] and this state appears to be catalytically relevant under all conditions canvassed,[8b] including with TfOH and Cp^*_2Co as the acid/reductant combination (Table S11). An alternative pathway to form $[(P_3^B)Fe{\equiv}N]^+$ under these milder conditions is shown in Scheme 1**C**, **D** via the known cationic hydrazido $[(P_3^B)Fe(NNH_2)]^+$.[12] We estimate the reduction potential of this species to be ≥ -1.2 V based on the alkyl congener (Fig. S32), and thus $[(P_3^B)Fe(N_2)]^-$ (or its oxidized congener $(P_3^B)Fe(N_2)$) is a sufficiently strong reductant to produce $(P_3^B)Fe(NNH_2)$ from $[(P_3^B)Fe(NNH_2)]^+$. The viability of this pathway is demonstrated by a low temperature protonation experiment of $[(P_3^B)Fe(N_2)]^-$ with excess TfOH (i.e. no exogenous reductant), which produced appreciable quantities of $[(P_3^B)Fe{\equiv}N]^+$ (~20%) and NH_3 (34(3)%) along with competitive oxidation to $(P_3^B)Fe(OTf)$. The same reaction sequence is thermodynamically-accessible under turnover conditions using Cp^*_2Co as the terminal source of reducing equivalents. Other routes to $[(P_3^B)Fe{\equiv}N]^+$ via metallocene-mediated proton-coupled electron transfer reactions are also conceivable.[8c]

In the transformation from $[(P_3^B)Fe(N_2)]^{2-}$ to $[(P_3^B)Fe{\equiv}N]^+$, the Fe center spans six formal oxidation states, from d^{10} Fe(−II) to d^4 Fe(IV). However, these formal assignments do not account for Z-

type Fe-to-B σ-backbonding,[20] in addition to π-backbonding with the phosphines. Indeed, the presence of pre-edge transitions in the XANES spectrum of $[(P_3^B)Fe(N_2)]^{2-}$, which is reproduced by TD-DFT, requires a physical oxidation state d^n with $n < 10$ (Fig. 2**A**, **B**). The physical oxidation state range of Fe is buffered by these soft electron-accepting interactions, which allow e^- to be stored in covalent Fe–B/P backbonding interactions until transferred to the N–N unit upon protonation. The three sequential H^+ transfers to the distal N atom of $[(P_3^B)Fe(N_2)]^{2-}$ to form $[(P_3^B)Fe{\equiv}N]^+$ and NH_3 result in a lengthening of the Fe–B distance by 0.61 Å (distances from DFT) and a lengthening of the average Fe–P distance by 0.07 Å (distances from EXAFS), reflecting loss of Fe–B/P covalency (Fig. 3**C**). Owing to the highly flexible Fe-borane interaction, which increases from 2.34 Å ($[(P_3^B)Fe(N_2)]^{2-}$) to 2.59 Å ($(P_3^B)Fe(NNH_2)$) to 2.95 Å ($[(P_3^B)Fe{\equiv}N]^+$), the valency of Fe is largely conserved as it distorts out of the P_3 plane to form π bonds with the NNH_2^{2-} and N^{3-} ions. This is reflected in the nearly constant sum of the bond orders about Fe for $[(P_3^B)Fe(N_2)]^{2-}$ (5.2), $(P_3^B)Fe(NNH_2)$ (4.7), and $[(P_3^B)Fe{\equiv}N]^+$ (4.8), a notion supported by the fact that the change in isomer shift (Δδ) is only 0.38 mm s^{-1} (0.06 mm s^{-1}/e^-). For comparison, Δδ is nearly 1 mm s^{-1} for a series of isostructural Fe complexes ranging over only five formal oxidation states (ca. 0.2 mm s^{-1}/e^-).[7c]

The demanding multi-electron process, $[(P_3^B)Fe^I]^+ + N_2 + 3H^+/3\,e^- \rightarrow [(P_3^B)Fe^{IV}{\equiv}N]^+ + NH_3$ (Scheme 1**C**, **D**), is thus facilitated by load-sharing of the reducing equivalents between Fe and the ligand. In this way, the redox behavior of the $(P_3^B)Fe$ unit crudely models that of a metallocluster, in which the potential range of multi-electron processes is compressed by delocalization of electrons/holes among many metals.[21] Analogy may also be made to the reduction of O_2 to ferryl (Fe^{IV}=O) and H_2O mediated by heme cofactors, in which the last reducing equivalent necessary to cleave the O–O bond is derived from the porphyrin and/or thiolate ligand (Scheme 1**A**).[2a] The generation of a terminal $Fe^{IV}{\equiv}N$ from the reductive protonation of N_2 validates the previous hypothesis that a mononuclear Fe N_2 fixation catalyst can support the range of *formal* oxidation states required to stabilize both π-acidic N_2 and π-basic N^{3-} ligands.[3b] However, this transformation is facilitated by covalency with the ligand atoms, which buffers the *physical* oxidation state range of Fe in this system, a feature of potential relevance to biological N_2 fixation, where the multimetallic [FeS] assembly may serve a similar function.[9]

ASSOCIATED CONTENT

Supporting Information

Experimental procedures, characterization data, and computational models. The Supporting Information is available free of charge on the ACS Publications website at http://pubs.acs.org.

AUTHOR INFORMATION

Corresponding Author

m.green@uci.edu
jpeters@caltech.edu

ACKNOWLEDGMENT

We thank M. Latimer, E. Nelson, C. Krest, C. Miller, and K. Mittra for assistance with synchrotron measurements, L. Henling and M. Takase for assistance with XRD, D. VanderVelde for assistance with NMR, and T. J. Del Castillo for assistance with catalytic experiments. This work was supported by the Resnick Sustainability Institute at Caltech (Graduate Fellowship, N.B.T.), as well as the NIH (GM 070757). Use of the Stanford Synchrotron Radiation Lightsource, SLAC National Accelerator Laboratory, is supported by the U.S. Department of Energy, Office of Science, Office of Basic Energy Sciences under Contract No. DE-AC02-76SF00515. The SSRL Structural Molecular Biology Program is supported by the DOE Office of Biological and Environmental Research, and by the National Institutes of Health, National Institute of General Medical Sciences (including P41GM103393). The contents of this publication are solely the responsibility of the authors and do not necessarily represent the official views of NIGMS or NIH.

REFERENCES

1. Hohenberger, J.; Ray, K.; Meyer, K. *Nat. Commun.* **2012,** *3*, 720.
2. (a) Poulos, T. L. *Chem. Rev.* **2014,** *114*, 3919-3962; (b) Que, L. *Acc. Chem. Res.* **2007,** *40*, 493-500.
3. (a) Betley, T. A.; Peters, J. C. *J. Am. Chem. Soc.* **2004,** *126*, 6252-6254; (b) Hendrich, M. P.; Gunderson, W.; Behan, R. K.; Green, M. T.; Mehn, M. P.; Betley, T. A.; Lu, C. C.; Peters, J. C. *Proc. Nat. Acad. Sci.* **2006,** *103*, 17107-17112.
4. Chatt, J.; Dilworth, J. R.; Richards, R. L. *Chem. Rev.* **1978,** *78*, 589-625.
5. (a) Yandulov, D. V.; Schrock, R. R. *J. Am. Chem. Soc.* **2002,** *124*, 6252-6253; (b) Yandulov, D. V.; Schrock, R. R. *Science* **2003,** *301*, 76-78; (c) Tanaka, H.; Arashiba, K.; Kuriyama, S.; Sasada, A.; Nakajima, K.; Yoshizawa, K.; Nishibayashi, Y. *Nat. Commun.* **2014,** *5*.
6. Scepaniak, J. J.; Vogel, C. A.; Khusniyarov, M. M.; Heinemann, F. W.; Meyer, K.; Smith, J. M. *Science* **2011,** *331*, 1049-1052.
7. (a) Wagner, W. D.; Nakamoto, K. *J. Am. Chem. Soc.* **1988,** *110*, 4044-4045; (b) Meyer, K.; Bill, E.; Mienert, B.; Weyhermüller, T.; Wieghardt, K. *J. Am. Chem. Soc.* **1999,** *121*, 4859-4876; (c) Berry, J. F.; Bill, E.; Bothe, E.; George, S. D.; Mienert, B.; Neese, F.; Wieghardt, K. *Science* **2006,** *312*, 1937-1941; (d) Vogel, C.; Heinemann, F. W.; Sutter, J.; Anthon, C.; Meyer, K. *Angew. Chem., Int. Ed.* **2008,** *47*, 2681-2684; (e) Scepaniak, J. J.; Fulton, M. D.; Bontchev, R. P.; Duesler, E. N.; Kirk, M. L.; Smith, J. M. *J. Am. Chem. Soc.* **2008,** *130*, 10515-10517; (f) Rodriguez, M. M.; Bill, E.; Brennessel, W. W.; Holland, P. L. *Science* **2011,** *334*, 780-783; (g) Aliaga-Alcade, Núria; DeBeer George, S.; Mienert, B.; Bill, E; Wieghardt, K.; Neese, F. *Angew. Chem. Int. Ed.* **2005**, *44*, 2908-2912; (h) Sabenya, G.; Lázaro, L.; Gamba, I.; Martin-Diaconescu, V.; Andris, E.; Weyhermüller, T.; Neese, F.; Roithova, J.; Bill, E.; Lloret-Fillol, J.; Costas, M. *J. Am. Chem. Soc.* **2017**, *139*, 9168-9177.
8. (a) Anderson, J. S.; Rittle, J.; Peters, J. C. *Nature* **2013,** *501*, 84-7; (b) Del Castillo, T. J.; Thompson, N. B.; Peters, J. C. *J. Am. Chem. Soc.* **2016,** *138*, 5341-5350; (c) Chalkley, M. J.; Del Castillo, T. J.; Matson, B. D.; Roddy, J. P.; Peters, J. C. *ACS Central Science* **2017,** *3*, 217-223.
9. Seefeldt, L. C.; Hoffman, B. M.; Dean, D. R. *Annu. Rev. Biochem* **2009,** *78*, 701-722.
10. Rittle, J.; Peters, J. C. *J. Am. Chem. Soc.* **2016,** *138*, 4243-4248.
11. Moret, M.-E.; Peters, J. C. *Angew. Chem. Int. Ed.* **2011,** *50*, 2063-2067.
12. Anderson, J. S.; Cutsail, G. E., III; Rittle, J.; Connor, B. A.; Gunderson, W. A.; Zhang, L.; Hoffman, B. M.; Peters, J. C. *J. Am. Chem. Soc.* **2015,** *137*, 7803-7809.
13. Lee, Y. H.; Mankad, N. P.; Peters, J. C. *Nat. Chem.* **2010,** *2*, 558-565.
14. Gütlich, P.; Bill, E.; Trautwein, A. X., *Mössbauer Spectroscopy and Transition Metal Chemistry*. Springer Berlin Heidelberg: New York, 2011.
15. Rudd, P. A.; Liu, S.; Planas, N.; Bill, E.; Gagliardi, L.; Lu, C. C. *Angew. Chem. Int. Ed.* **2013,** *52*, 4449-4452.
16. Rohde, J.-U.; Betley, T. A.; Jackson, T. A.; Saouma, C. T.; Peters, J. C.; Que, L., Jr. *Inorg. Chem.* **2007,** *46*, 5720-5726.
17. Weng, T.-C.; Hsieh, W.-Y.; Uffelman, E. S.; Gordon-Wylie, S. W.; Collins, T. J.; Pecoraro, V. L.; Penner-Hahn, J. E. *J. Am. Chem. Soc.* **2004,** *126*, 8070-8071.
18. Westre, T. E.; Kennepohl, P.; DeWitt, J. G.; Hedman, B.; Hodgson, K. O.; Solomon, E. I. *J. Am. Chem. Soc.* **1997,** *119*, 6297-6314.
19. Anderson, J. S.; Moret, M. E.; Peters, J. C. *J. Am. Chem. Soc.* **2013,** *135*, 534-537.
20. Bouhadir, G.; Bourissou, D. *Chem. Soc. Rev.* **2016,** *45*, 1065-1079.
21. Hernández Sánchez, R.; Zheng, S.-L.; Betley, T. A. *J. Am. Chem. Soc.* **2015,** *137*, 11126-11143.

TOC GRAPHIC